# Carbonic anhydrase IX (CA9) modulates tumor-associated cell migration and invasion

**Hye-Jin Shin[1], Seung Bae Rho[1], Dae Chul Jung[1], Inn-Oc Han[2], Eok-Soo Oh[3] and Joo-Young Kim[1,*]**

[1]Research Institute and Hospital, National Cancer Center, Goyang 410-769, Korea
[2]College of Medicine, Department of Physiology and Biophysics, Inha University, Incheon 402-751, Korea
[3]Department of Life Sciences, Division of Life and Pharmaceutical Sciences and the Center for Cell Signaling and Drug Discovery Research, Ewha Womans University, Seoul 120-750, Korea
*Author for correspondence (jooyoungcasa@ncc.re.kr)

*Accepted 12 November 2010*
*Journal of Cell Science 124, 1077-1087*

*doi:10.1242/jcs.072207*

## Summary

Expression of carbonic anhydrase IX (CA9) was shown to be strongly involved in high incidences of metastasis and poor prognosis in various human tumors. In this study, we investigated the possible role for CA9 in tumor metastases in vitro, using a gene transfection tool in the human cervical carcinoma cell line C33A. Gene expression profiling of CA9-transfected cells (C33A/CA9) and vector-transfected cells (C33A/Mock) was investigated by DNA microarray. The biological functions of differentially expressed genes between the C33A/CA9 and C33A/Mock cells included cell growth, regulation of cell–cell and cell–extracellular matrix adhesion and cytoskeletal organization. Immunofluorescent stain and Matrigel culture showed cytoskeletal remodeling, disassembled focal adhesion, weakened cell-cell adhesion and increased motility in C33A/CA9 cells. These invasive and metastatic phenotypes were associated with Rho-GTPase-related epithelial-mesenchymal transition. Inhibition of the Rho/Rho kinase pathway by a ROCK inhibitor (Y27632) and si-Rho (short interference RNA against RhoA) showed that Rho-GTPase signaling was involved in cellular morphologic and migratory changes. The effect of CA9 on Rho-GTPase signaling was also confirmed by silencing CA9 expression. Our results suggest that CA9 overexpression induces weakening of cell adhesions and augmented cell motility by aberrant Rho-GTPase signal transduction. Our study shows an underlying mechanism of CA9-related enhanced metastatic potential of tumor cells.

**Key words:** Carbonic anhydrase IX (CA9), Migration, Invasion, Cell adhesion, Cytoskeleton, Epithelial-mesenchymal transition (EMT), Rho, Rho kinase

## Introduction

Carbonic anhydrases (CAs) are a family of zinc metalloenzymes that catalyze the rapid reversible hydration of carbon dioxide to bicarbonate and protons (Svastova et al., 2003). At least 13 human CA isoenzymes that exhibit catalytic activity are distributed in various human organs, tissues and subcellular compartments, playing an important role in essential cellular processes such as pHe and pHi regulation, secretion of electrolytes, respiration and biosynthetic reactions that require $CO_2$ and $HCO_3^-$ as substrates (e.g. lipogenesis, gluconeogenesis and ureagenesis) (Thiry et al., 2006; Zatovicova et al., 2005). CA9, the only transmembrane CA isoenzyme with an extracellular active site and an $NH_2$-terminal proteoglycan-like region, is also implicated in cell adhesion as well as in acid-base balancing and intercellular communication (Robertson et al., 2004; Svastova et al., 2003). CA9 expression is most notably induced by hypoxic conditions under tight regulation by hypoxia-inducible factor 1 alpha (HIF1-α) and has been shown to be distributed at perinecrotic areas in neoplastic tissues (Giatromanolaki et al., 2001; Wykoff et al., 2000). Such finding suggests that extracellular acidification by CA9 might be closely associated tumorigenic transformation, breakdown of the extracellular matrix, induction of cell growth factors and protease activation in a hypoxic microenvironment (Thiry et al., 2006). In our previous study, tumors with high expression of CA9 in primary tumor tissues were associated with a higher incidence of lymph node metastasis and poor prognosis (Kim et al., 2006; Lee et al., 2007). When expression of CA9 was examined in primary cervical tumor tissues and their surgically-dissected matching lymph nodes (LN), the primary tumors that showed high CA9 expression also showed high CA9 expression in the matching metastatic LNs, which suggests that the CA9-expressing clones in tumors are metastatic clones (Lee et al., 2007).

Metastasis is one of the hallmarks of malignancy and the most common cause of death in cancer patients (Yang et al., 2004). The metastatic process comprises a complex series of steps, which starts with a loss of cell–cell adhesion, an increase in cell motility and augmented invasiveness into the surrounding tissues. This process involves an epithelial-mesenchymal transition (EMT), which contributes to the dissemination of epithelial cancer cells (Imai et al., 2003; Yang et al., 2004).

To search for the key regulators of metastasis related to CA9 expression under hypoxic conditions, we established a cell line that constitutively expresses CA9 using the C33A human cervical cancer cell line (Shin et al., 2008). We then further investigated differentially expressed gene profiles in CA9-transfected C33A cervix cancer cells (C33A/CA9) compared with vector-only-transfected cells (C33A/Mock) (Shin et al., 2008), using the Affymetrix Human Genome U133 Plus gene chip assay. Because our previous studies consistently revealed the high metastatic potential in tumors where CA9 is overexpressed (Kim et al., 2006; Lee et al., 2007), we focused on the gene ontology categories related to metastatic phenotypes. The respective gene functions included cellular cytoskeletal remodeling, focal adhesion, cell-cell adhesion and migration. In this study, a series of genes that were

Journal of Cell Science

differentially expressed more than 2-fold, which are related to the above-mentioned cell functions, were investigated. As genes involved in Rho-GTP-kinase pathway were also differentially expressed between the two cell lines, the roles for other selected genes were investigated in association with Rho/Rho kinase activity.

## Results

### Differentially expressed gene profiles in a CA9-transfected C33A cell line

As a result of DNA microarray analysis using Human U133 Plus 2.0 ChIP, a total of 463 genes were shown to be differentially expressed between the C33A/CA9 and the C33A/Mock cells, of which 228 were upregulated and 235 were downregulated by more than twofold. Among those genes, 148 upregulated and 136 downregulated genes had known biological functions. Biological data mining showed that most of the genes were associated with cell growth, cell morphology and cell motility. Further exploration was made for the genes related to cytoskeleton organization and cell adhesion. Genes regulating cytoskeletal organization and cell adhesion (ARHGDIA, restin, vimentin, paxillin, talin, etc.) were upregulated in C33A/CA9 cells compared with the C33A/Mock cells, whereas the genes involved in Rho-GTPase activation and the retention of the extracellular matrix (THBS1, TIMP2, FGD6, CDC42EP3, etc.) were downregulated in the C33A/CA9 as compared with the C33A/Mock cells (Table 1). Expression of these genes was confirmed by reverse-transcriptase PCR (RT-PCR) and quantitative RT-PCR. The correlation between gene expression profiles and quantitative RT-PCR was ascertained in seven selected genes including CA9 (Fig. 1). The same results were confirmed using polyclonal C33A/Mock and polyclonal C33A/CA9 cells in order to demonstrate that the changes observed in C33A/CA9 cells were not due to different clonality (data not shown).

### Effect of CA9 on formation of actin stress fiber and focal adhesion

On the basis of microarray analysis, it was decided to investigate the role for CA9 in actin cytoskeleton reorganization and cellular adhesion. C33A/CA9 and C33A/Mock cells were plated onto Matrigel basement membrane matrix extracted from the Engelbreth-Holm-Swarm (EHS) mouse sarcoma, a tumor rich in extracellular

**Table 1. The list of differentially expressed genes in C33A/CA9 cells compared with in C33A/Mock cells**

| Gene ontology | Gene ID number | Gene name | Fold change (FC) |
|---|---|---|---|
| Carbon compound metabolism | NM_001216 | Carbonic anhydrase IX (CA9) | 5.14 |
| Cell growth; regulation of cell size | NM_002045 | Growth associated protein 43 | 7.61 |
| | NM_001423 | Epithelial membrane protein 1 (EMP1) | 6.89 |
| | AI809967 | SHC (Src homology 2 domain containing) transforming protein 1 | 2.43 |
| | NM_003377 | Vascular endothelial growth factor B | 2.01 |
| | NM_006747 | Signal-induced proliferation-associated gene 1 | 2.07 |
| | AF051344 | Latent transforming growth factor beta binding protein | 2.08 |
| Cell adhesion | AI571798 | Rho GDP dissociation inhibitor (GDI) alpha (ARHGDIA) | 4.07 |
| | AF498927 | Rho GDP dissociation inhibitor (GDI) beta (ARHGDIB) | 2.08 |
| | NM_004343 | Calreticulin | 3.95 |
| | NM_001464 | A disintegrin and metalloproteinase domain 2 (fertilin beta) (ADAM2) | 5.14 |
| Regulation of signal transduction | NM_012242 | Dickkopf homolog 1(Xenopus laevis) (DKK1) | 13.63 |
| | NM_016431 | Mitogen-activated protein kinase 8 interacting protein | 2.02 |
| | AB016929 | Regulator of G-protein signaling 11 | 2.01 |
| | AA775681 | Chromosome 1 ORF 139 | 2.04 |
| | BE045549 | Mindbomb homolog 2 (Drosophila) | 2.32 |
| | U79264 | Zic family member 1 (odd-paired homolog, Drosophila) | 2.10 |
| | D86862 | Paxillin | 2.24 |
| | AF188179 | Guanine nucleotide binding protein (G protein), gamma 8 | 2.73 |
| Intermediate filament; structural constituent of cytoskeleton | BF673049 | Restin (Reed-Steinberg cell-expressed intermediate filament) | 2.06 |
| | NM_021076 | Neurofilament, heavy polypeptide 200 kDa | 4.20 |
| | AI922599 | Vimentin | 2.53 |
| | S62137 | Dopamine receptor D2 | 2.04 |
| | NM_006950 | Synapsin 1 | 2.16 |
| | NM_006289 | Talin 1 | 2.57 |
| | NM_004877 | Glia maturation factor, gamma | 2.30 |
| | NM_022359 | Phosphodiesterase 4D interacting protein | 3.01 |
| | NM_003282 | Troponin 1, skeletal, fast | 2.16 |
| | AA912711 | Erythrocyte membrane protein band 4.1-like 1 | 3.00 |
| | AI358867 | Apolipoprotein E | 2.04 |
| | AF143684 | Myosin IXB | 2.06 |
| | NM_006790 | Titin immunoglobulin domain protein (Myotilin) | 6.30 |
| | NM_005775 | Vinexin beta (SH3-containing adaptor molecule-1) | 2.69 |
| Adhesive glycoprotein | BF055462 | Thrombospondin 1 (THBS 1) | 0.25 |
| Blood coagulation | BF983379 | CD59 antigen p18-20 (CD59) | 0.46 |
| Protease inhibitor | BE968786 | Tissue inhibitor of metalloproteinase 2 (TIMP2) | 0.46 |
| Regulation of body fluid | J03225 | Tissue factor pathway inhibitor (lipoprotein-associated coagulation inhibitor) | 0.39 |
| Enzyme inhibitor | NM_001262 | Cyclin-dependent kinase inhibitor 2C | 0.43 |
| Actin binding; protein binding | AF010314 | Ectodermal-neural cortex (with BTB-like domain) (ENC1) | 0.17 |
| | NM_005010 | Neuronal cell adhesion molecule (NRCAM) | 0.43 |
| Guanyl-nucleotide exchange factor activity | AL136842 | CDC42 effector protein (Rho GTPase binding) 3 (CDC42 EP3) | 0.45 |
| | NM_018351 | FYVE, Rho GEF and PH domain containing 6 (FGD6) | 0.40 |
| Mannosidase activity | NM_002372 | Mannosidase, alpha, class 2A, member 1 (MAN2A1) | 0.40 |

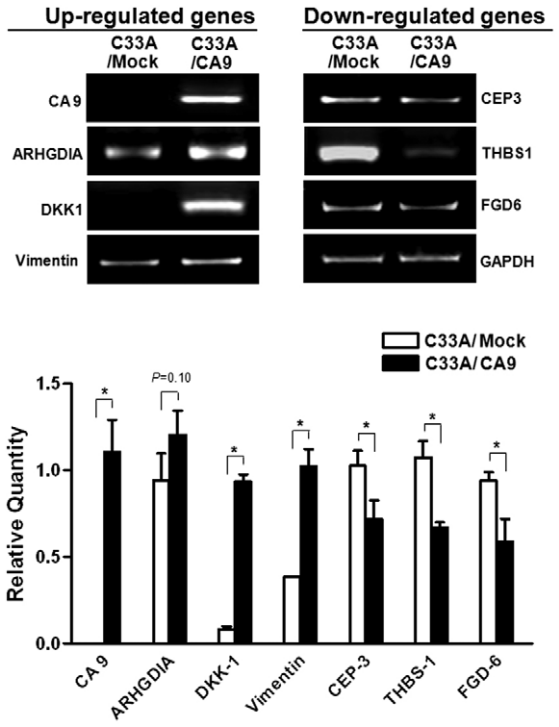


**Fig. 1. The list of differentially expressed genes in C33A/CA9 and C33A/Mock cells.** Differentially expressed genes were selected on the basis of fold-change in CA9-overexpressed (C33A/CA9) cells versus vector-transfected control (C33A/Mock) cells. Gene expressions were confirmed by RT-PCR and quantitative RT-PCR. The relative quantity for each molecule was normalized with GAPDH, which was used as an internal control. Each bar represents the mean (plus standard error) of four independent experiments. **P*<0.05.

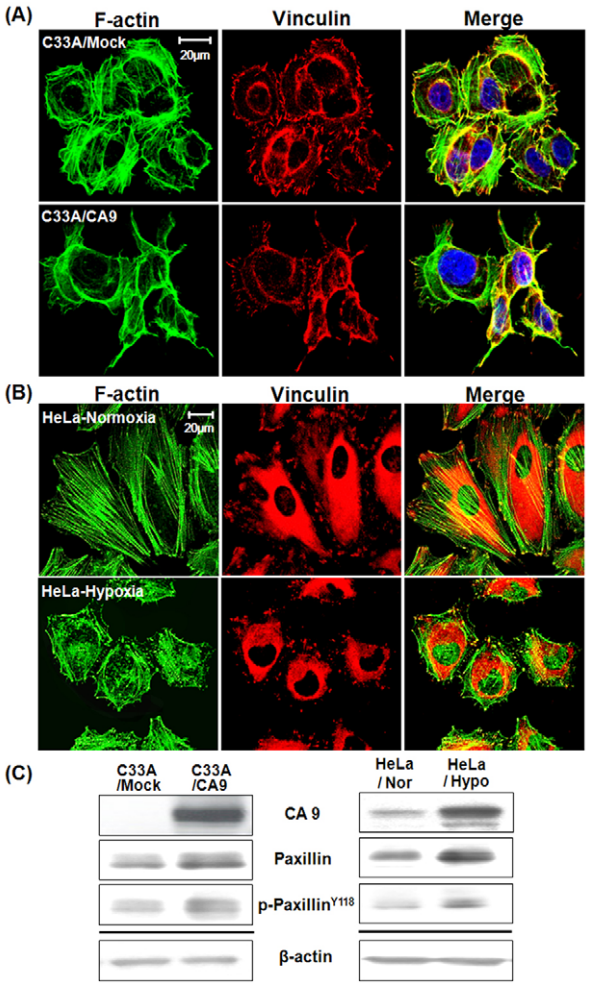


**Fig. 2. Reorganization of actin cytoskeleton and alteration of focal adhesion induced by CA9 overexpression.** (**A**) C33A/CA9 and C33A/Mock cells were incubated on glass slides pre-coated with BD Matrigel Matrix with the cultured medium for 24 hours. Actin filaments (green) of cytoskeleton, vinculin (red) of focal adhesion complex and nuclear DNA (blue) were stained with phalloidin conjugated with Alexa 488, anti-vinculin antibody labeled with Alexa 594 and DAPI, respectively. (**B**) HeLa cells were cultured under normoxic (20% $O_2$) and hypoxic (0.1% $O_2$) conditions and were stained in the same manner as in A. (**C**) Cells grown as described above were harvested and CA9 expression was confirmed using M75 monoclonal antibody. Expression and phosphorylation of paxillin was examined by immunoblotting, using the indicated antibodies (anti-paxillin, anti-pPaxillin$^{Y118}$). β-actin was used as a loading control.

matrix proteins. When the cells were stained with phalloidin conjugated with Alexa 488 and anti-vinculin antibody labeled with Alexa 594 to visualize actin stress fibers and focal adhesion complexes, it was observed that the C33A/CA9 cells had relatively thicker and shorter actin bundles restricted to the cellular periphery and actin-rich membrane protrusions at leading edges. The number of focal adhesion complexes visualized by vinculin were higher and more prominent in C33A/Mock cells, whereas vinculin expression was more concentrated at the end of the membrane protrusion complexes and appeared to be diminished in number and size in most of the C33A/CA9 cells (Fig. 2A,B). This pattern was very similar to the morphological changes of HeLa cells in which CA9-expression was greatly stimulated by hypoxic conditions (Fig. 2B) (Shin et al., 2008). The expression and tyrosine phosphorylation of paxillin, a major regulator in organization and function of focal adhesions, were assessed by western blot analysis (Fig. 2C). Interestingly, both the expression level and phosphorylation level at Tyr118 of paxillin were increased in C33A/CA9 cells, which supported the increase in paxillin expression in microarray analysis (Table 1). Supplementary material Fig. S1 shows the basal level of CA9 expression and its change under hypoxic conditions in C33A cell lines. Tissues from the invasive cervix carcinomas with negative and strong expression of CA9, respectively, were selected and examined for CA9 expression by western blot and immunohistochemical staining.

## CA9 is associated with increased cell migration and invasion

Unlike C33A/Mock cells, which mostly showed a general flattened shape with a number of actin stress fibers transversing the entire cell body, C33A/CA9 cells showed cytoskeletal changes leading to a stellate morphology. C33A/Mock cells maintained steady focal adhesions; however, C33A/CA9 cells showed miniature focal adhesions on Matrigel-coated plates (Fig. 2A,B). In addition to this, C33A/CA9 cells grown in the 3D Matrigel culture showed severely compromised cell-to-cell adhesion and increased cell motility, which was indicated by the appearance of loose clumps with multiple budding of the cells into the surrounding Matrigel

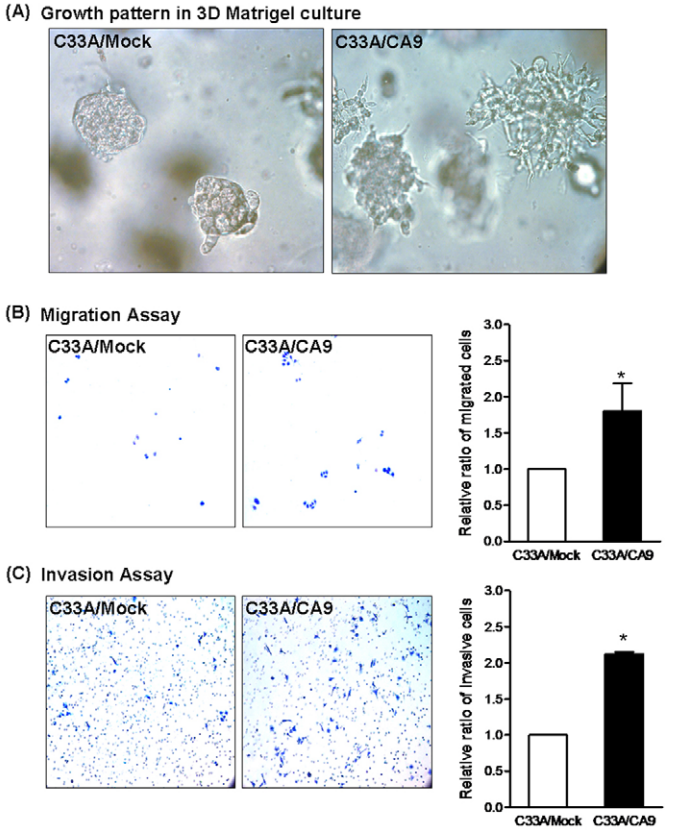


**Fig. 3. Increased invasive and metastatic ability with CA9 overexpression.** (**A**) C33A/CA9 and C33A/Mock cells were suspended as single cells and were cultured in Matrigel for two weeks. Images of the spheroid colonies were acquired using a light microscope (100× magnification). (**B**,**C**) Migratory and invasive ability of two cell lines were examined using Transwell chambers with or without Matrigel coating. The cells migrating through the filters were enumerated and the relative ratio of migrating C33A/CA9 cells to migrating C33A/Mock cells was determined. Each illustration shows the typical image and each bar represents the mean (plus standard error) of six independent experiments (*, $P<0.05$ compared with C33A/Mock cells).

stroma. This was in contrast to the C33A/Mock cell culture where densely aggregated clumps of cells were observed (Fig. 3A). Similar results were obtained in a Transwell chamber assay performed to quantify the migratory and invasive cells (Fig. 3B,C). Each bar represents the mean (plus standard error) of six independent experiments. Migrating and invading cells were significantly promoted in C33A/CA9 cells compared with C33A/Mock cells (unpaired *t*-test, $P=0.0305$ and 0.0375 for the migration and invasion assay, respectively; Fig. 3B,C).

### Rho-GTPase signaling is involved in cellular morphologic and migratory changes

To further clarify the molecular mechanism underlying these phenotypes associated with CA9, we focused on Rho-GTPases, which are known as key regulators of actin cytoskeleton formation and cellular adhesion through their interaction with downstream effector proteins (Ren et al., 1999). Rho-GTPase receives upstream signals through regulators such as GDP–GTP exchange protein (GEP), GDP dissociation inhibitor (GDI) and GTPase activating protein (GAP), which modulates shuttling between the inactive GDP-bound and the active GTP-bound forms, thus transmitting

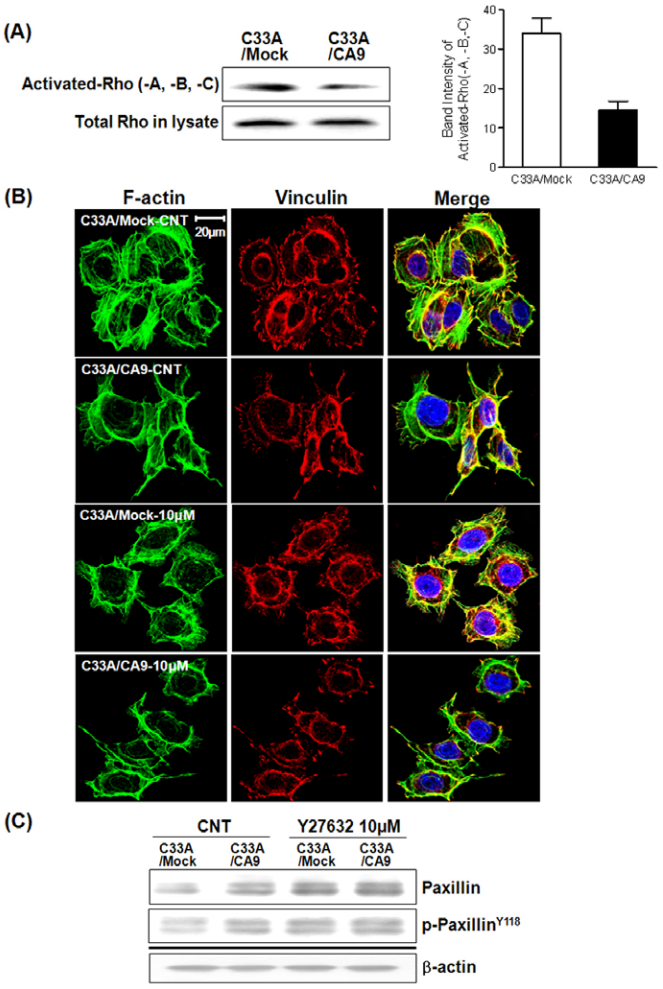


**Fig. 4. Rho-GTPase activity and changes in cytoskeletal structure and focal adhesion with CA9 overexpression.** (**A**) The amount of GTP-bound Rho-GTPase was compared between two cells by GST-RBD pull-down assay. Band intensity of activated RhoA/B/C-GTPases was quantified by image software, Multi Gauge, V3.0 (FUJIFILM). (**B**) Changes in actin cytoskeleton and focal adhesions subsequent to blocking the Rho downstream with ROCK inhibitor (Y27632) were observed by immunofluorescence analysis. C33A/Mock and C33A/CA9 cells were plated as in Fig. 2A and treated with a final 10 μM Y27632 after 3 hours. Actin filaments, vinculins and nuclear DNA were stained as green, red and blue signal, respectively. (**C**) Total lysates from two cell line cultures treated with or without 10 μM Y27632 as described in B were used for immunoblotting for expression and phosphorylation of paxillin. β-actin was used as a loading control.

signals to downstream effectors such as Rho kinase (ROCK) (Kim et al., 2007; Ren et al., 1999). By examining microarray data, we observed that GDI, which interacts with the GDP-bound form and prevents it from being converted to the GTP-bound form, was increased, whereas CDC42EP3 [also known as small GTPase effector protein 3 (CEP3)] was decreased in C33A/CA9 cells (Table 1; Fig. 1). Western blot analysis also showed a reduction of the GTP-bound active form in C33A/CA9 cells (Fig. 4A), supporting the gene expression result. Furthermore, we investigated changes in cell morphology, adhesions and migration after inhibition of Rho signaling by blocking ROCK with the selective inhibitor Y27632 (Biosource). In this experiment, cells received a

treatment of 10 μM ROCK inhibitor Y27632 on a Matrigel matrix for 20 hours. The effect of Y27632 was more profoundly observed in C33A/Mock cells, changing the shape of the cells into stellate morphology with formation of thicker and shorter actin stress fibers compared with the pre-treatment cell (C33A/Mock-CNT) morphology. Focal adhesions of the cells to the stroma were shown only in the leading edge of the cell–stroma contact and were disassembled overall (Fig. 4B). The expression and tyrosine phosphorylation of paxillin were remarkably increased in C33A/Mock cells after Y27632 treatment (Fig. 4C). In addition, the tight cell-to-cell contact that was observed in 3D Matrigel culture of C33A/Mock cells was remarkably diminished and many budding daughter clumps were observed with Y27632 treatment (Fig. 5A). Migrating and invading cells were also significantly increased after Y27632 treatment compared with C33A/Mock-CNT cells (Fig. 5B,C). Each bar represents the mean (plus standard error) of six independent experiments. However, cell adhesion and motility between the C33A/CA9-CNT cells and the C33A/CA9 cells treated with Y27632 was not significantly different, suggesting that the C33A/CA9 cells were not significantly influenced by Y27632 treatment (Fig. 5A–C) and that there was constitutively low Rho kinase activity in this cell line.

### CA9-induced Rho inactivation leads to epithelial–mesenchymal transition

According to the previous reports, Rho-GTPases are implicated in EMT owing to their involvement in dissociation of cell adhesions and cytoskeletal remodeling (Patel et al., 2005; Tumbarello et al., 2005). Therefore, we examined the expression of epithelial markers such as E-cadherin and α-catenin and mesenchymal markers such as vimentin and N-cadherin by western blot analysis. The expression of E-cadherin and α-catenin was stronger in C33A/Mock cells than in C33A/CA9 cells and its expression was reduced by treatment with Y27632 in C33A/Mock cells. By contrast, the expression of mesenchymal proteins, particularly vimentin was strongly increased in C33A/CA9 cells compared with C33A/Mock cells (Fig. 6C). After Y27632 treatment, the expression of mesenchymal markers was reversed in C33A/Mock cells; however, C33A/CA9 cells did not show changes after the same treatment, suggesting that the EMT process is strongly activated by constitutively high expression of CA9 and low Rho-GTPase activity in this cell line. The quantitative measurement of proteins related to EMT was also observed by immunofluorescent staining of the same proteins. E-cadherin was generally distributed in the cell membrane of C33A/Mock cells, whereas it was diffusely distributed in low levels within the cytoplasm and not in the cell membrane of C33A/CA9 cells. The Y27632-treated C33A/Mock cells showed weakening and changes of distribution in E-cadherin with a dramatic change in cell shape. In C33A/CA9 cells, vimentin filaments appeared to be extended along the cell periphery to the nucleus and were distributed more on the leading region. After Y27632 treatment, a similar appearance to C33A/CA9 cells was also observed in C33A/Mock cells (Fig. 6A,B). The observation that Y27632-induced Rho signaling inhibition in C33A/Mock cells leads to a phenotypic change similar to that of the C33A/CA9 cells in terms of increased migratory activity and increased mesenchymal protein expression suggests that the increased migratory and invasive phenotype of C33A/CA9 cells are attributed to the aberrant Rho signaling by Rho-GTPase inactivation. The phenotypic characteristics observed by the treatment with Y27632 were also reproduced by siRNA-mediated Rho A silencing (Fig. 7A,B),

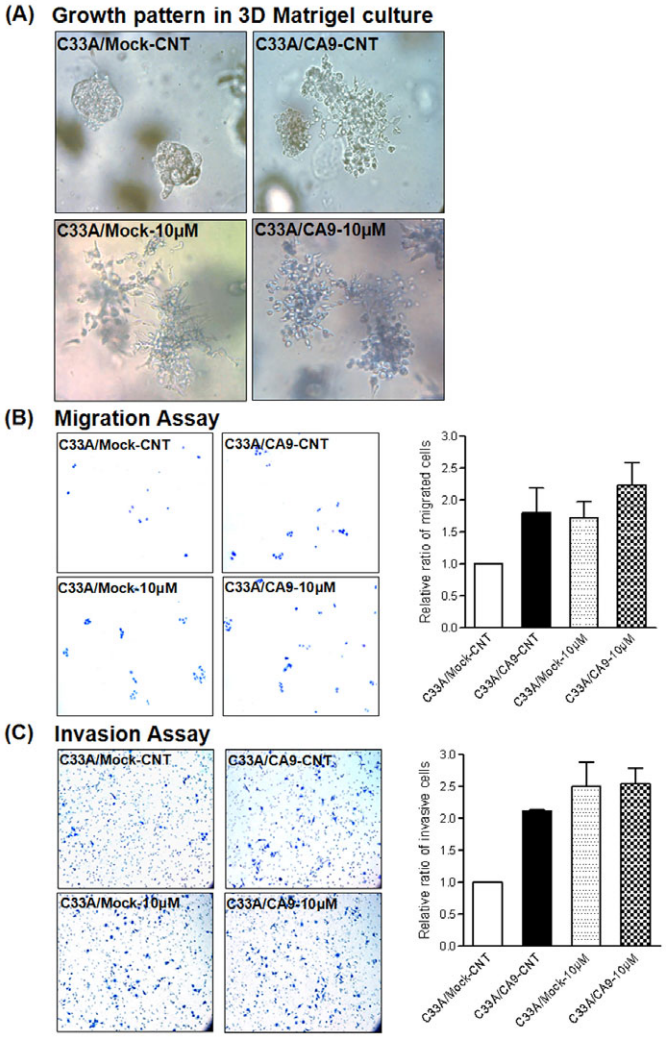


**Fig. 5. Migratory and invasive potential improved with Rho-GTPase inactivation in C33A/CA9 cells.** (**A**) C33A/Mock and C33A/CA9 cells were cultured in Matrigel for 8 days, as in Fig. 3A and were treated with final 10 μM Y27632 at this time to start cells clumping. Y27632 inhibitor was treated two more times and the cells were observed using a light microscope (100× magnification). (**B**,**C**) Migrating and invading ability of the cells were examined as in Fig. 3B and 3C. Cells were seeded onto respective Transwell chambers and were treated with 10 μM Y27632 3 hours after seeding. Each figure illustrates the typical image obtained and each bar represents the mean (plus standard error) of six independent experiments.

which confirms the role for decreased Rho activity in phenotypic changes of C33A/CA9 cells. To demonstrate whether the above results were induced by CA9 overexpression, we performed a siRNA-mediated CA9 silencing experiment (Fig. 8). As a result, we confirmed that activity of Rho, but not the other small GTPases such as ras-related C3 botulinum toxin substrate 1 (RAC1) and cell division control protein 42 (CDC42), is strongly influenced by CA9 expression. Changes in paxillin and EMT markers shown in C33A/CA9 cells were restored to a similar level to that of C33A/Mock cells after silencing of CA9 expression (Fig. 8A,D). The migratory and invasive ability of C33A/CA9 cells was nearly as low as that of C33A/Mock cells with inhibition of CA9 by siRNA (Fig. 8B,C).

### CA9 directly interacts with DKK1

To understand the working mechanism of CA9, we investigated CA9 binding proteins using a yeast two-hybrid interaction assay system. One prominent protein identified was dickkopf homolog 1 (DKK1), which was also detected in microarray analysis with a 13.6-fold increase in C33A/CA9 cells compared with C33A/Mock cells. Positive interaction was observed by using both cell growth and β-galactosidase activity (Fig. 9A). As shown in Fig. 9A, positive β-galactosidase activity was observed in the CA9–DKK1 system, whereas very little β-galactosidase activity was observed in the CA9–empty-vector system. To further confirm the direct interaction between CA9 and DKK1 that we observed in the yeast two-hybrid system, we performed co-immunoprecipitation (Co-IP). pcDNA3.1–DKK1 was co-immunoprecipitated with pcDNA and Flag-CA9, whereas no interaction was observed between pcDNA3.1 (vector only) and pcDNA3.1 with Flag–CA9 (Fig. 9B). An immunoblotting assay using anti-CA9 antibody confirmed that an equal amount of CA9 was precipitated in both samples (Fig. 9B). The interaction of the two proteins was also revealed by Co-IP of endogenous CA9 and DKK1 (Fig. 9C). These results clearly indicated that CA9 directly interacts with DKK1 at a physiological level.

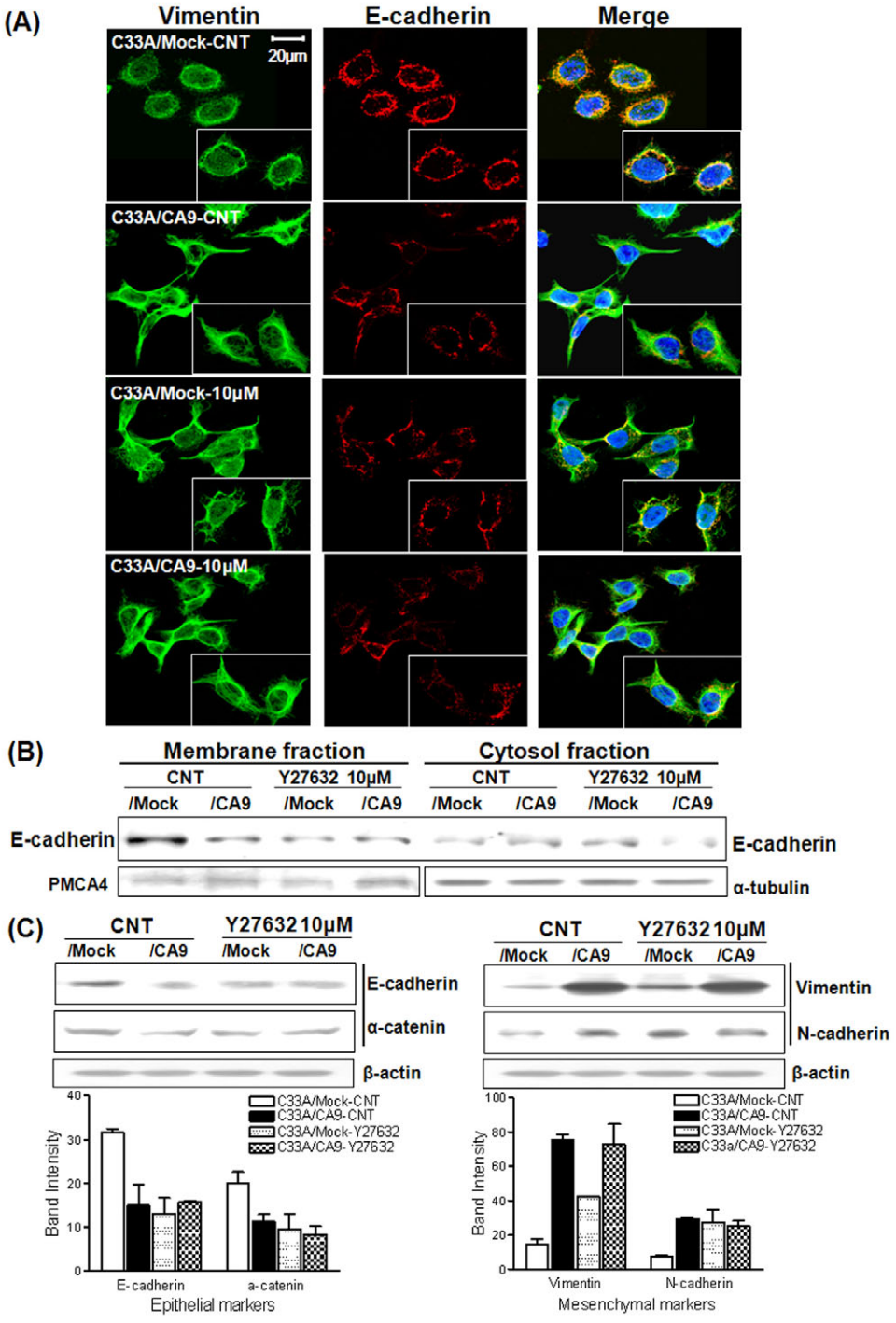


**Fig. 6. The role of Rho-GTPase signaling in the EMT process.** (**A**) The expression and localization of E-cadherin and vimentin were examined by immunofluorescence analysis. Prepared under the same conditions as in Fig. 4B, the cells were stained for E-cadherin (red) and vimentin (green) with Alexa-594- and Alexa-488-labeled secondary antibodies, respectively. (**B**) Thirty micrograms of the membranous and cytoplasmic fraction of proteins obtained from the cells were loaded and the expression of E-cadherin was analyzed by western blotting. PMCA4 (plasma membrane calcium ATPase 4) and α-tubulin were used as controls for membranous and cytoplasmic proteins, respectively. (**C**) Expression of epithelial markers (E-cadherin and α-catenin) and mesenchymal markers (vimentin and N-cadherin) were examined by western blot in both C33A/Mock and C33A/CA9 cells, with or without Y27632 treatment. β-actin was used as a loading control. Band intensity from western blot images was quantified by Multi Gauge V3.0 (FUJIFILM). Each bar represents the mean (plus standard error).

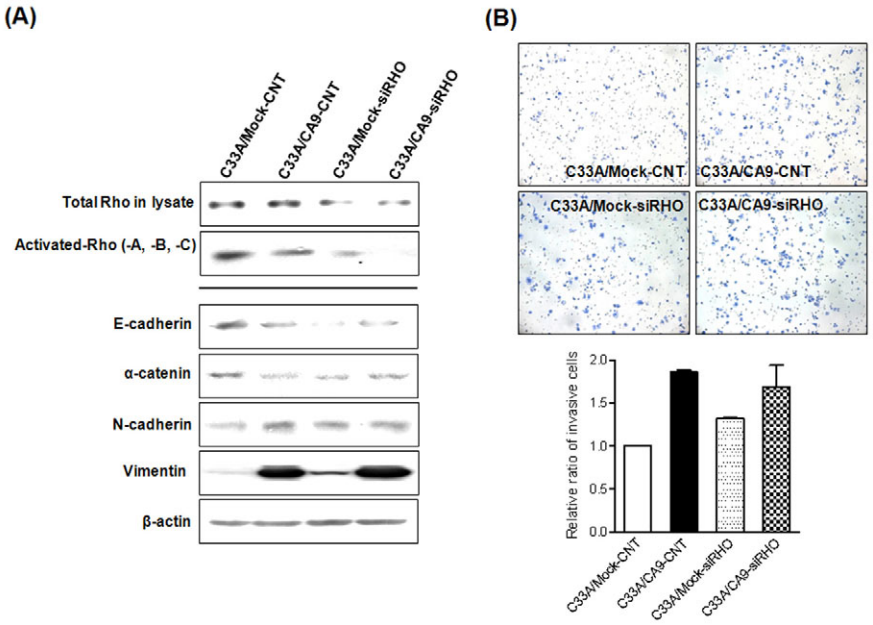


**Fig. 7. Rho signaling is crucial to form the migratory phenotypes.** The role of Rho signaling was validated using two types of siRNAs against RhoA at a concentration of 25 nM. A double-stranded non-specific siRNA was used as a negative control (CNT). (**A**) Block efficiency of si-Rho and quantitative changes of EMT markers were analyzed by western blot. β-actin was used as a loading control. (**B**) An invasion assay using Transwell chambers with Matrigel coating was repeated six times. The cells migrating through the filters were enumerated and the relative ratio of invasive cells was normalized by the number of migrating C33A/Mock-CNT cells. Illustrations show the typical images and the bars represent the mean (plus standard error).

## Discussion

Recent studies have reported the important role for the tumor microenvironment in association with invasive and aggressive phenotypes (Mueller and Fusenig, 2004; Quaranta and Giannelli, 2003). Destabilization of intercellular contacts, increased cell motility, altered tissue morphogenesis and remodeling, acidification of extracellular pH and increased activity of tissue proteinase involved in the breakdown of the extracellular matrix are known to be required for the process of metastasis to occur. CA9 has not only an enzyme activity to induce the acidification of extracellular pH, but also physical function to perturb tight intercellular contacts linked to the cytoskeleton through competition with E-cadherin in binding with β-catenin (Mueller and Fusenig, 2004; Svastova et al., 2003). In this study, we showed that the transcriptional level of many genes, and hence aberrant signal transduction related to cell adhesion and cytoskeletal organization, can be induced by overexpression of CA9. Immunofluorescent staining of actin filaments and focal adhesion complex proteins revealed dramatic changes in CA9-transfected cells that were similar to the pattern of HeLa cells exposed to a concentration of 0.1% oxygen, thus indicating that the observed changes in CA9-overexpressing C33A cells are one of the underlying mechanisms of increased metastatic potential of the cancer cells under a hypoxic microenvironment.

As genes related to Rho/Rho kinase signal transduction pathway were changed at the same time in CA9-expressing cells and because Rho-GTPases and Rho kinase activity are known to regulate a variety of cellular functions such as cytoskeletal reorganization, cell-cell adhesion, cell cycle progression and motility, we investigated whether this pathway was the underlying mechanism of CA9-related phenotypic changes. Rho-GTPases, including the classical Rho, RAC and CDC42, regulate the above-mentioned cellular functions through upstream pathways, cycling between an inactive GDP-bound form and an active GTP-bound form under regulation by GEFs, GAPs and GDIs (Guo et al., 2006; Ridley, 2001; Togawa et al., 1999), and downstream pathways carried by Rho kinase and p21-activated kinases. Upon active GTP-bound state targeting to the membrane fraction, GTPases transmit signals from cell-surface receptors to intercellular target molecules via several different pathways. Specifically, Rho stimulates the formation of actin stress fiber and focal adhesion, whereas CDC42 activation triggers the extension of filopodia and RAC controls growth-factor-stimulated membrane ruffling and formation of lamellipodia. Recently, Rho-GTPase-directed mechanisms were suggested to play a key role in EMT (Holtje et al., 2005; Patel et al., 2005) through the extensive crosstalk between the three GTPases (Holtje et al., 2005; Nimnual et al., 2003; Yamaguchi et al., 2001), altering the activation status of the respective GTPases. In addition to this, previous studies showed that inactivation of RhoA either by direct inhibition with exoenzyme C3 or by blocking downstream targets such as ROCK with Y27632 contributed to enhanced migration and EMT while maintaining expression of active RAC1 and CDC42 (Holtje et al., 2005; Patel et al., 2005). Our experimental results are also in line with these observation because migratory and invasive ability were enhanced with the induction of mesenchymal markers in C33A/Mock cells when Rho-GTPase downstream signaling was blocked by Y27632 and specific siRNAs against RhoA. In addition, recent studies showed that Tyr31/118 phosphorylation of paxillin competes with p190RhoGAP for binding to p120RasGAP and provided evidence that p190RhoGAP freed from p120RasGAP efficiently suppressed RhoA activity during cell adhesion to the ECM (Jagadeeswaran et al., 2008; Tsubouchi et al., 2002; Zaidel-Bar et al., 2007). Paxillin, a focal adhesion scaffolding protein, not only plays a crucial role in dynamic changes of focal adhesion and binding to other focal adhesion proteins such as FAK, vinculin, talin and tensin, but also affects the regulation of cell spreading, motility and muscle differentiation. The latter functions are known to be a result of the direct interaction with multiple structural and signaling proteins such as tubulin, p120RasGAP, PKL, PTP-PEST, SRC, CRK and CSK (Iwasaki et al., 2002; Jagadeeswaran et al., 2008; Tumbarello et al., 2005; Zaidel-Bar et al., 2007). A link between tyrosine phosphorylation of paxillin and Rho activity was observed in our study. Our results showed that the suppression of Rho signaling induced tyrosine phosphorylation of paxillin and subsequently activated paxillin-transmitted signals, which promote dynamic adhesion turnover and cell migration.

The previous study of Pastorekova et al. (Svastova et al., 2003) showed a relationship between CA9 and E-cadherin in cell adhesion, whereas we showed the effect of CA9 on Rho/ROCK signaling transduction and EMT in the current study. Tracing the upstream signal in these relationships, we found that CA9 directly binds to the secreted protein DKK1, which is known as one of the transcriptional target genes along with vimentin, fibroblast growth factor 20 (FGF20) in the Wnt/β-catenin/TCF signaling pathway (Chamorro et al., 2005; Kuang et al., 2009; Schlessinger et al., 2009; Orsulic et al., 1999). Interaction of CA9 and DKK1 might

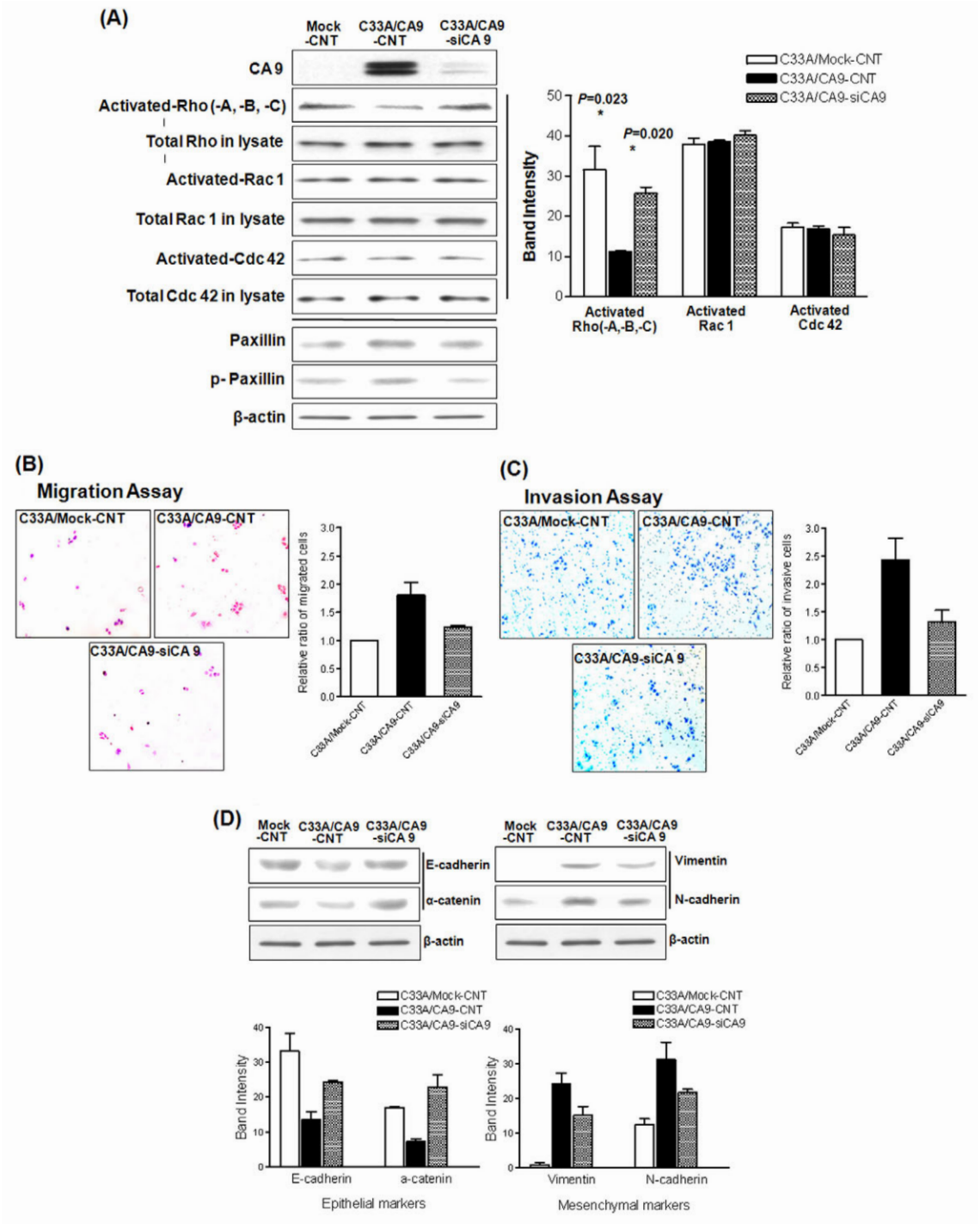


**Fig. 8. The effect of CA9 on migration and invasion is validated by siRNAs against CA9.** (**A**) Block efficiency of si-CA9 was validated by western blot. A double-stranded non-specific siRNA was used as a negative control (CNT). C33A/CA9 cells were transfected with 150 nM siRNA against CA9 for 24 hours and then were transferred onto Matrigel-coated dishes. After incubation for 24 hours, total cell lysates were analyzed for small GTPases such as Rho, RAC, CDC42 and paxillin using a pull-down assay and western blot analysis. Band intensity from western blot images was quantified by Multi Gauge V3.0. (**B**,**C**) At 24 hours post-transfection, the cells were prepared for migration and invasion assays as in Fig. 5B and C. (**D**) Cells were prepared as in Fig. 8A and were analyzed for EMT markers by western blot analysis. After silencing of CA9 expression, epithelial markers increased in expression, whereas mesenchymal markers decreased in C33A/CA9 cells. Each bar represents the mean (plus standard error).

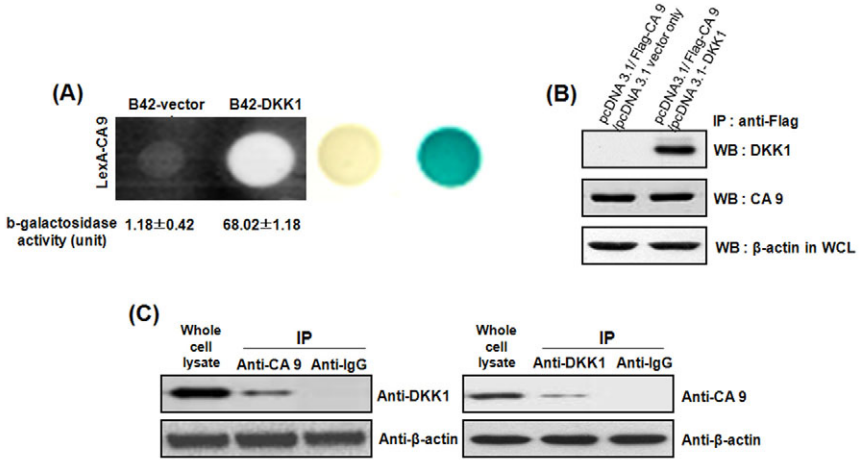


**Fig. 9. Interaction analysis between human CA9 and DKK1.** (**A**) Interaction of CA9 with the indicated proteins using the yeast two-hybrid assay system. Positive interactions are indicated by the formation of blue colonies on medium containing X-gal. Binding activity of CA9 and DKK1 activity was measured by adding ONPG. Data were expressed as the mean ± s.e.m. (**B**) Coimmunoprecipitation of pcDNA3.1– Flag-CA9 and pcDNA3.1–DKK1. Proteins immunoprecipitated with anti-Flag antibody were analyzed by western blot analysis with anti-DKK1 antibody. Data shown are representative of three independent experiments. (**C**) Coimmunoprecipitation between endogenous CA9 and DKK1 displays the presence of an interaction of the two proteins.

induce a conformational change of CA9 and prevent GDP-Rho from moving to the coupled receptor on the cell membrane, which in turn blocks interaction with Rho-specific effectors such as GEFs and GAPs. Although future studies will be required to fully elucidate the mechanism underlying CA9–DKK1 interaction and CA9–DKK1-mediated RhoA/ROCK signaling pathway, our present findings provide important new insights into tumor-associated cell migration and invasion. Overall, we suggest that overexpression of CA9 contributes to increasing metastatic potential through interference with the Rho/ROCK signaling pathway, which might be associated with CA9–DKK1 interaction and transcriptional regulation of the β-catenin signaling pathway.

## Materials and Methods

### Cell culture and stable transfection of C33A cells

The human cervical cancer cell line C33A (ATCC number HTB-31) was stably transfected with either full-length human CA9 cDNA cloned into the pcDNA3 vector or empty vector control (Shin et al., 2008). Transfected polyclonal cell populations were selected for growth in the presence of 250 μg/ml G418 (GIBCO-BRL, Gaithersburg, MD) for 3 weeks. Selected monoclonal CA9-transfected cells (C33A/CA9) and vector-only-transfected cells (C33A/Mock) were tested for expression of CA9 as previously described by real-time PCR and western blot analysis (Shin et al., 2008). M75, the monoclonal antibody for CA9, was a kind gift from Silvia Pastorekova (Slovak Academy of Sciences, Slovakia). Cells were maintained at 5% $CO_2$ in RPMI (for C33A cells) or MEM (for HeLa cells) medium with 10% fetal bovine serum supplemented with 1% streptomycin and penicillin.

### RNA isolation and microarray analysis

Total RNA was extracted from the cells using a TRIzol (Invitrogen, Carlsbad, CA) method, followed by cleanup with the RNeasy Mini Kit isolation method (Qiagen GmbH, Hilden, Germany). Microarray was performed using 5 μg total RNA and Affymetrix Human Genome U133 Plus 2.0 arrays (Affymetrix, Santa Clara, CA) containing ~54,675 total probes and 63 control probes. We performed synthesis of biotin-labeled cRNA from total RNA samples and hybridization on Affymetix arrays, according to the Affymetrix standard protocols. After staining, intensities were determined with a GeneChip Scanner 3000 (Affymetrix). Scanned data were pre-processed with an RMA (robust multi-array average) procedure using only perfect match (PM) probe intensities for background adjustment (Irizarry et al., 2003). RMA was preceded by quantile normalization (Bolstad et al., 2003) and median polish summarization of PM intensities (Irizarry et al., 2003). The differentially expressed genes with over 2-fold change were selected to analyze the biological inter-relationship. Genplex software, version 3.0 (ISTECH Inc., Goyang-si, Republic of Korea), was used for the biological data mining. Specification of the many gene annotations was also supplemented by further online database searches. Microarray data have been deposited in the Gene Expression Omnibus (http://www.ncbi.nlm.nih.gov/geo/) and are accessible through Gene Expression Omnibus series number GSE20569.

### Reverse transcriptase-PCR (RT-PCR) and quantitative RT-PCR

For validation of microarray data, a total of seven genes associated with cell growth, morphology and motility, including CA9, were selected for RT-PCR and quantitative RT-PCR. The RT-PCR and quantitative RT-PCR were carried out as previously described (Kim et al., 2006). The primer sequences used for RT-PCR were as follows: CA9 (Forward) 5′-TAAGCAGCTCCACACCCTCT-3′, (Reverse) 5′-TCTCATCTGCACAAGGAACG-3′; ARHGDIA (Forward) 5′-CTTGATG-GTGAGATTCCACT-3′, (Reverse) 5′-TGAAGTACATCAGCCATACG-3′; DKK1 (Forward) 5′-CACTGATGAGTACTGCGCTA-3′, (Reverse) 5′-CAGAA-CCTTCTTGTCCTTTG-3′; vimentin (Forward) 5′-GAGAGGAAGCCGAAA-ACACC-3′, (Reverse) 5′-GCTTGGAAACATCCACATCG-3′; CEF3 (Forward) 5′-TCAGGAGAAAAGCAGTCTGT-3′, (Reverse) 5′-GAGAGGGACTC-CTCTGACTT-3′; THBS1 (Forward) 5′-CTGGACAACTGTCCCTATGT-3′, (Reverse) 5′-AAATCGGTCTCACTGATGTC-3′; FGD6 (Forward) 5′-CCCA-GACATCAGCATTCCAG-3′, (Reverse) 5′-AGCTACTGCATCCCGGAAAT-3′; GAPDH (Forward) 5′-TCATTGACCTCAACTACATGGT-3′. TaqMan pre-designed assays of each gene were provided by Applied Biosystems (Foster City, CA) for quantitative RT-PCR. Assay IDs are as follows: ARHGDIA, Hs00976924 g1; DKK1, Hs00183740 m1; vimentin, Hs00958116 m1; THBS1, Hs00962908 m1; FGD6, Hs00217947 m1; CDC42EP3, Hs00377831 m1.

### Immunofluorescence analysis

Cells were attached onto glass slides coated with 500 μg/ml BD Matrigel Basement Membrane Matrix (BD Biosciences, San Jose, CA) for 24 hours, kept under the medium and cultured with respective cell lines for 4 days and then were fixed in 3.7% formaldehyde for 20 minutes at room temperature. The cells were permeabilized with 0.1% Triton X-100 for 5 minutes at room temperature and were treated with 1% BSA in TBST (TBS containing 0.2% Tween 20) to block nonspecific reaction. Sequential incubation of primary antibody (Upstate Biotechnology, Waltham, MA) and Alexa fluorescence-conjugated secondary antibody (Molecular Probes, Eugene, OR) was performed with DNA stained with DAPI (Molecular Probes). For hypoxic experiments for HeLa cells, the cells were incubated under hypoxic (0.1% $O_2$) and normoxic (20% $O_2$) conditions for 18 hours before immunofluorescent staining. The stained cells were mounted with DAKO mounting medium (DAKO Corporation, Carpinteria, CA) and were examined using a confocal laser scanning microscope (Zeiss LSM 510 META, Car Zeiss Microimaging, Inc., Thornwood, NY) at 400× magnification. The primary antibodies used were vinculin (Sigma-Aldrich, St Louis, MO), E-cadherin (BD Transduction Laboratories, San Jose, CA), vimentin (BD Pharmingen, San Diego, CA), and phalloidin (Molecular Probes).

### Subcellular fractionation

To prepare the differential extraction of proteins from monolayer-cultured cells according to their subcellular localization, we used the ProteoExtract Subcellular Proteome Extraction Kit (Calbiochem, San Diego, CA). Cells cultured on 500 μg/ml Matrigel-coated 100 mm plates were lysed and subcellular components were separated as recommended by the manufacturer. The cytosol fraction and membrane fraction proteins were analyzed by western blotting. PMCA4 (plasma membrane calcium ATPase 4) and α-tubulin were used as internal controls for plasma membrane and cytoplasm proteins, respectively.

### Western blot analysis and antibodies

Cells ($1\times10^6$) were cultured on 500 μg/ml Matrigel-coated 100 mm plates under the same culture conditions used for immunofluorescent staining. The cells were washed twice with cold PBS prior to solubilization in cold lysis buffer containing 50 mM Tris-HCl (pH 8.0), 0.25 M sodium chloride, 1% NP-40, 1% Triton X-100, 2 mM $CaCl_2$, 1 mM PMSF and protease inhibitor cocktail (Sigma) for 40 minutes at 4°C. Lysates were denatured and reduced with 5× SDS sample buffer. Protein samples (~10-30 μg each) were separated by 8% (N-cadherin, E-cadherin and α-catenin) or

12% (CA9, vimentin, paxillin, RhoA/B/C, RAC1, CDC42 and β-actin) SDS-PAGE and transferred to a Hybond–ECL nitrocellulose membrane (GE Healthcare, Little Chalfont, Buckinghamshire, UK). Membranes were blocked with 3% bovine serum albumin in TBST and incubated with primary antibodies in blocking solution at 4°C overnight. After washing with TBST, horseradish-peroxidase-conjugated secondary antibodies (Cell Signaling Technology, Beverly, MA) were applied and the blots were developed by the Enhanced Chemiluminescence Detection System (GE Healthcare Life Sciences). The antibodies used were CA9, a kind donation from Silvia Pastorekova (Institute of Virology, Slovak Academy of Sciences, Slovak Republic), β-actin (Abcam, Cambridge, UK), vimentin (BD Pharmingen), N-cadherin, E-cadherin, α-catenin (BD Transduction), paxillin (Upstate Biotechnology, Lake Placid, NY), pPaxillin$^{Y118}$ (Invitrogen), α-tubulin (Abcam) and PMCA4 (Santa Cruz Biotechnology, Santa Cruz, CA).

### Three-dimensional multicellular spheroid culture using Matrigel Basement Membrane Matrix

Matrigel Basement Membrane Matrix (BD Biosciences) was thawed and mixed homogeneously as recommended by the supplier. Single cells ($5\times10^3$) were suspended in 600 µl Matrigel using cooled pipettes and were allowed to gel on a 24-well plate for 30 minutes at 37°C. The cells embedded in thick gel were incubated for 4 days in culture medium containing an equal volume of fresh growth medium and the medium used to culture the cells in order to magnify the expected effects of CA9 enzymatic activity. After two weeks, the Matrigel was fixed and stained with Diff-Quik (Kokusai-Shiyaku, Kobe, Japan) solution. Images of the cells grown in 3D matrix were acquired using a light microscope (100× magnification; Olympus, Center Valley, PA) with a digital camera system (Prog-Res C14; Jenoptik, Jena, Germany).

### Migration assay

Cell migration assays were performed using 6.5 mm Transwell chambers (Corning Costar Corp., Cambridge, MA) containing polycarbonate membrane (8 µm pore size). Media cultured with C33A/Mock and C33A/CA9 cells for 4 days was added to their respective lower chambers and was used to dilute the cells to a concentration of $5\times10^5$ cells per 0.5 ml. The cell suspension was added to each upper chamber and incubated at 37°C for 16 hours. Cells that migrated to the bottom of the plate through the membrane were fixed and stained with Diff-Quik solution (Kokusai-Shiyaku) and enumerated using a light microscope (40× or 100× magnification; Olympus). Each experiment was performed in triplicate wells and repeated two times. Each bar represents the mean (plus standard error) of six independent experiments.

### Invasion assay

A Matrigel Invasion Chamber (BD Biosciences) was hydrated with 500 µl serum-free medium added to both lower and upper chambers for at least 2 hours at 37°C in a $CO_2$ incubator. After rehydration of the Matrigel, the lower chamber was replaced with media cultured for 4 days and the upper chamber was filled with cell suspension diluted at concentration of $4\times10^4$ cells per 0.5 ml. The invasion chamber plate was incubated for 24 hours. Unmigrated cells on the upper side of the Matrigel-coated insert were removed with cotton swabs and the cells invading through the Matrigel were fixed and stained with Diff-Quik solution (Suzuki et al., 2005). The number of cells that invaded the Matrigel layer was quantified following the same protocol used for the migration assays.

### Rho-GTPase activity assay

An activity assay for RhoA/B/C, small GTPases, was conducted with the Rho Activation Assay Kit (Upstate) according to the manufacturer's instructions. In brief, the GST-rhotekin-RBD (Rho binding domain) fusion protein of the Rho Activation Assay Kit was used to specifically precipitate GTP-Rho, the active form of Rho-GTPase. The GST-RBD was incubated with total cell lysate at 4°C for 1 hour. The GTP-Rho pulled down from the lysate was detected by western blot analysis using anti-RhoA/B/C antibody. Like the preceding pull-down assay, the activity of RAS-related C3 botulinum toxin substrate 1 (RAC1) and cell division control protein 42 (CDC42) was examined using the GST-PAK1 PBD (p21 binding domain of human PAK1) reagent, anti-RAC1 and anti-CDC42 antibody (Upstate).

### Silencing of gene expression by short interference RNA

Target siRNAs for silencing of human CA9 and RhoA were obtained from Qiagen. The sequences of the si-CA9 sense strand were 5′-GGCUGCUGGUGACAUCCUATT-3′ and 5′-ACCUGAAGUUAAGCCUAAATT-3′. The siRNAs against RhoA are HP Validated siRNA products (SIO2654211 and SIO2654267). A double-stranded non-specific siRNA (Qiagen) was used as a negative control. The siRNA transfection was conducted with Lipofectamine 2000 reagent (Invitrogen) according to the manufacturer's instructions. Cells plated for 24 hours were transfected with 150 nM of si-CA9 (two kinds of si-CA9 RNA were mixed at 75 nM each) or with 50 nM of si-RhoA (two kinds of si-RhoA RNA were mixed at 25 nM each). At 24 hours after transfection, the cells were prepared for the migration and invasion assays, the Rho-GTPase activity assay and western blot analysis.

### Yeast two-hybrid analysis

For bait construction with human CA9, cDNA encoding full-length human CA9 was subcloned into the *Eco*RI and *Xho*I restriction enzyme sites of the pLexA cloning vector. The resulting plasmid, pLexA-CA9, was introduced into yeast strain EGY48 [*MATa*, *his3*, *trp1*, *ura3-52*, *leu2::pLeu2-LexAop6*/*pSH18-34* (*LexAop-lacZ* reporter)] by a modified lithium acetate method (Rho et al., 1996). Human DKK1 was fused by cloning the cDNA fragments into the *Eco*RI and *Xho*I restriction enzyme sites of pJG4-5 to generate B42 fusion proteins (Clontech, Palo Alto, CA). The cDNAs encoding B42 fusion proteins were introduced into the competent yeast cells that already contained pLexA-CA9 and the transformants were selected for the tryptophan prototrophy (plasmid marker) on synthetic medium (Ura, His, Trp) containing 2% (w/v) glucose. The binding activity of the interaction between CA9 and DKK1 was confirmed by measuring the relative expression level of β-galactosidase. β-galactosidase activity was determined according to the previously described method (Rho et al., 1996).

### Co-immunoprecipitation (Co-IP)

To identify the protein interacting partner and targets of CA9, gene-encoding human *CA9* was subcloned into pcDNA3.1–Flag (Invitrogen) with *Eco*RI and *Xho*I (pcDNA3.1–Flag-*CA9*). The human *DKK1* gene was ligated into pcDNA3.1 (Invitrogen) using *Eco*RI and *Xho*I (pcDNA3.1-*DKK1*). For IP, pcDNA3.1–Flag-*CA9* and pcDNA3.1-*DKK1* expression plasmids were cotransfected into HEK 293 cells using Fugene transfection reagent (Roche). Lysates were then incubated with anti-Flag antibody (Santa Cruz Biotechnology) and precipitated with protein-A-agarose (GE Healthcare Life Sciences). The precipitated proteins were resolved by SDS gel electrophoresis, transferred onto Immobilon P membrane (Millipore, Billerica, MA) and subjected to immunoblot analysis with anti-DKK1 antibody (Abnova, Walnut, CA) or anti-CA9 antibody using the ECL system (GE Healthcare Life Sciences).

We thank Y. K. Sung in the Kyungpook National University School of Medicine for providing the *DKK1* gene used in our supplementary experiment. This work was supported by the National Cancer Center Grant 1010870-1, Goyang, Republic of Korea. Neither actual nor potential conflicts of interest exist.

Supplementary material available online at
http://jcs.biologists.org/cgi/content/full/124/7/1077/DC1

## References

**Bolstad, B. M., Irizarry, R. A., Astrand, M. and Speed, T. P.** (2003). A comparison of normalization methods for high density oligonucleotide array data based on variance and bias. *Bioinformatics* **19**, 185-193.

**Chamorro, M. N., Schwartz, D. R., Vonica, A., Brivanlou, A. H., Cho, K. R. and Varmus, H. E.** (2005). FGF-20 and DKK1 are transcriptional targets of beta-catenin and FGF-20 is implicated in cancer and development. *EMBO J.* **24**, 73-84.

**Giatromanolaki, A., Koukourakis, M. I., Sivridis, E., Pastorek, J., Wykoff, C. C., Gatter, K. C. and Harris, A. L.** (2001). Expression of hypoxia-inducible carbonic anhydrase-9 relates to angiogenic pathways and independently to poor outcome in non-small cell lung cancer. *Cancer Res.* **61**, 7992-7998.

**Guo, F., Debidda, M., Yang, L., Williams, D. A. and Zheng, Y.** (2006). Genetic deletion of Rac1 GTPase reveals its critical role in actin stress fiber formation and focal adhesion complex assembly. *J. Biol. Chem.* **281**, 18652-18659.

**Holtje, M., Hoffmann, A., Hofmann, F., Mucke, C., Grosse, G., Van Rooijen, N., Kettenmann, H., Just, I. and Ahnert-Hilger, G.** (2005). Role of Rho GTPase in astrocyte morphology and migratory response during in vitro wound healing. *J. Neurochem.* **95**, 1237-1248.

**Imai, T., Horiuchi, A., Wang, C., Oka, K., Ohira, S., Nikaido, T. and Konishi, I.** (2003). Hypoxia attenuates the expression of E-cadherin via up-regulation of SNAIL in ovarian carcinoma cells. *Am. J. Pathol.* **163**, 1437-1447.

**Irizarry, R. A., Bolstad, B. M., Collin, F., Cope, L. M., Hobbs, B. and Speed, T. P.** (2003). Summaries of Affymetrix GeneChip probe level data. *Nucleic Acids Res.* **31**, e15.

**Iwasaki, T., Nakata, A., Mukai, M., Shinkai, K., Yano, H., Sabe, H., Schaefer, E., Tatsuta, M., Tsujimura, T., Terada, N. et al.** (2002). Involvement of phosphorylation of Tyr-31 and Tyr-118 of paxillin in MM1 cancer cell migration. *Int. J. Cancer* **97**, 330-335.

**Jagadeeswaran, R., Surawska, H., Krishnaswamy, S., Janamanchi, V., Mackinnon, A. C., Seiwert, T. Y., Loganathan, S., Kanteti, R., Reichman, T., Nallasura, V. et al.** (2008). Paxillin is a target for somatic mutations in lung cancer: implications for cell growth and invasion. *Cancer Res.* **68**, 132-142.

**Kuang, H. B., Miao, C. L., Guo, W. X., Peng, S., Cao, Y. J. and Duan, E. K.** (2009). Dickkopf-1 enhances migration of HEK293 cell by beta-catenin/E-cadherin degradation. *Front. Biosci.* **14**, 2212-2220.

**Kim, J. Y., Shin, H. J., Kim, T. H., Cho, K. H., Shin, K. H., Kim, B. K., Roh, J. W., Lee, S., Park, S. Y., Hwang, Y. J. et al.** (2006). Tumor-associated carbonic anhydrases are linked to metastases in primary cervical cancer. *J. Cancer Res. Clin. Oncol.* **132**, 302-308.

**Kim, T. Y., Lee, J. W., Kim, H. P., Jong, H. S., Jung, M. and Bang, Y. J.** (2007). DLC-1, a GTPase-activating protein for Rho, is associated with cell proliferation, morphology, and migration in human hepatocellular carcinoma. *Biochem. Biophys. Res. Commun.* **355**, 72-77.

**Lee, S., Shin, H. J., Han, I. O., Hong, E. K., Park, S. Y., Roh, J. W., Shin, K. H., Kim, T. H. and Kim, J. Y.** (2007). Tumor carbonic anhydrase 9 expression is associated with the presence of lymph node metastases in uterine cervical cancer. *Cancer Sci.* **98**, 329-333.

**Mueller, M. M. and Fusenig, N. E.** (2004). Friends or foes-bipolar effects of the tumour stroma in cancer. *Nat. Rev. Cancer* **4**, 839-849.

**Nimnual, A. S., Taylor, L. J. and Bar-Sagi, D.** (2003). Redox-dependent downregulation of Rho by Rac. *Nat. Cell Biol.* **5**, 236-241.

**Orsulic, S., Huber, O., Aberle, H., Arnold, S. and Kemler, R.** (1999). E-cadherin binding prevents β-catenin nuclear localization and β-catenin/LEF-1-mediated tranactivation. *J. Cell Sci.* **112**, 1237-1245.

**Patel, S., Takagi, K. I., Suzuki, J., Imaizumi, A., Kimura, T., Mason, R. M., Kamimura, T. and Zhang, Z.** (2005). RhoGTPase activation is a key step in renal epithelial mesenchymal transdifferentiation. *J. Am. Soc. Nephrol.* **16**, 1977-1984.

**Quaranta, V. and Giannelli, G.** (2003). Cancer invasion: watch your neighbourhood! *Tumori* **89**, 343-348.

**Ren, X. D., Kiosses, W. B. and Schwartz, M. A.** (1999). Regulation of the small GTP-binding protein Rho by cell adhesion and the cytoskeleton. *EMBO J.* **18**, 578-585.

**Ridley, A. J.** (2001). Rho GTPases and cell migration. *J. Cell Sci.* **114**, 2713-2722.

**Rho, S. B., Lee, K. H., Kim, J. W., Shiba, K., Jo, Y. J., Kim, S.** (1996). Interaction between human tRNA synthetases involves repeated sequence elements. *Proc. Natl. Acad. Sci. USA* **93**, 10128-10133.

**Robertson, N., Potter, C. and Harris, A. L.** (2004). Role of carbonic anhydrase IX in human tumor cell growth, survival, and invasion. *Cancer Res.* **64**, 6160-6165.

**Schlessinger, K., Hall, A. and Tolwinski, N.** (2009). Wnt signaling pathways meet Rho GTPases. *Genes Dev.* **23**, 265-277.

**Shin, H. J., Kim, J. Y., Yoo, C. W., Roberts, S. A., Lee, S., Choi, S. J., Lee, H. Y., Lee, D. H., Kim, T. H. and Cho, K. H.** (2008). Carbonic anhydrase 9 (CA9) expression in tumor cells enhances sensitivity to tirapazamine. *J. Cancer Res. Clin. Oncol.* **134**, 397-404.

**Suzuki, C., Daigo, Y., Ishikawa, N., Kato, T., Hayama, S., Ito, T., Tsuchiya, E. and Nakamura, Y.** (2005). ANLN plays a critical role in human lung carcinogenesis through the activation of RHOA and by involvement in the phosphoinositide 3-kinase/AKT pathway. *Cancer Res.* **65**, 11314-11325.

**Svastova, E., Zilka, N., Zat'ovicova, M., Gibadulinova, A., Ciampor, F., Pastorek, J. and Pastorekova, S.** (2003). Carbonic anhydrase IX reduces E-cadherin-mediated adhesion of MDCK cells via interaction with beta-catenin. *Exp. Cell Res.* **290**, 332-345.

**Thiry, A., Dogne, J. M., Masereel, B. and Supuran, C. T.** (2006). Targeting tumor-associated carbonic anhydrase IX in cancer therapy. *Trends Pharmacol. Sci.* **27**, 566-573.

**Togawa, A., Miyoshi, J., Ishizaki, H., Tanaka, M., Takakura, A., Nishioka, H., Yoshida, H., Doi, T., Mizoguchi, A., Matsuura, N. et al.** (1999). Progressive impairment of kidneys and reproductive organs in mice lacking Rho GDIalpha. *Oncogene* **18**, 5373-5380.

**Tsubouchi, A., Sakakura, J., Yagi, R., Mazaki, Y., Schaefer, E., Yano, H. and Sabe, H.** (2002). Localized suppression of RhoA activity by Tyr31/118-phosphorylated paxillin in cell adhesion and migration. *J. Cell Biol.* **159**, 673-683.

**Tumbarello, D. A., Brown, M. C., Hetey, S. E. and Turner, C. E.** (2005). Regulation of paxillin family members during epithelial-mesenchymal transformation: a putative role for paxillin delta. *J. Cell Sci.* **118**, 4849-4863.

**Wykoff, C. C., Beasley, N. J., Watson, P. H., Turner, K. J., Pastorek, J., Sibtain, A., Wilson, G. D., Turley, H., Talks, K. L., Maxwell, P. H. et al.** (2000). Hypoxia-inducible expression of tumor-associated carbonic anhydrases. *Cancer Res.* **60**, 7075-7083.

**Yamaguchi, Y., Katoh, H., Yasui, H., Mori, K. and Negishi, M.** (2001). RhoA inhibits the nerve growth factor-induced Rac1 activation through Rho-associated kinase-dependent pathway. *J. Biol. Chem.* **276**, 18977-18983.

**Yang, J., Mani, S. A., Donaher, J. L., Ramaswamy, S., Itzykson, R. A., Come, C., Savagner, P., Gitelman, I., Richardson, A. and Weinberg, R. A.** (2004). Twist, a master regulator of morphogenesis, plays an essential role in tumor metastasis. *Cell* **117**, 927-939.

**Zaidel-Bar, R., Milo, R., Kam, Z. and Geiger, B.** (2007). A paxillin tyrosine phosphorylation switch regulates the assembly and form of cell-matrix adhesions. *J. Cell Sci.* **120**, 137-148.

**Zatovicova, M., Sedlakova, O., Svastova, E., Ohradanova, A., Ciampor, F., Arribas, J., Pastorek, J. and Pastorekova, S.** (2005). Ectodomain shedding of the hypoxia-induced carbonic anhydrase IX is a metalloprotease-dependent process regulated by TACE/ADAM17. *Br. J. Cancer* **93**, 1267-1276.

Journal of Cell Science